Title
Surround Integration Organizes a Spatial Map during Active Sensation

Journal
Neuron, 94(6)

ISSN
0896-6273

Authors
Pluta, Scott R
Lyall, Evan H
Telian, Greg I
et al.

Publication Date
2017-06-01

DOI
10.1016/j.neuron.2017.04.026

Peer reviewed

HHS Public Access

Author manuscript

Neuron. Author manuscript; available in PMC 2018 June 21.

Published in final edited form as:

Neuron. 2017 June 21; 94(6): 1220–1233.e5. doi:10.1016/j.neuron.2017.04.026.

Surround integration organizes a spatial map during active sensation

Scott R. Pluta[1,4], **Evan H. Lyall**[2,4], **Greg I. Telian**[3], **Elena Ryapolova-Webb**[3], and **Hillel Adesnik**[1,3,5]

[1]Department of Molecular and Cell Biology, University of California, Berkeley, 94720

[2]Biophysics Graduate Group, University of California, Berkeley, 94720

[3]Helen Wills Neuroscience Institute, University of California, Berkeley, 94720

Abstract

During active sensation, sensors scan space in order to generate a representation of the outside world. However, since spatial coding in sensory systems is typically addressed by measuring receptive fields in a fixed, sensor-based coordinate frame, the cortical representation of scanned space is poorly understood. To address this question, we probed spatial coding in the rodent whisker system using a combination of two photon imaging and electrophysiology during active touch. We found that surround whiskers powerfully transform the cortical representation of scanned space. On the single neuron level, surround input profoundly alters response amplitude and modulates spatial preference in the cortex. On the population level, surround input organizes the spatial preference of neurons into a continuous map of the space swept out by the whiskers. These data demonstrate how spatial summation over a moving sensor array is critical to generating population codes of sensory space.

Introduction

Cortical neurons represent sensory space through topographic projections of the peripheral sense organs, creating maps of the physical world in the brain. Sensory coding through maps is thought to make both the structure and function of neural circuits more efficient (Knudsen et al., 1987). In passive systems, maps can be probed by systematically stimulating different parts of the sensor array and measuring the receptive fields of individual neurons. In many sensory systems, such as the retina, integration over the sensor array is critical for receptive field formation (Hartline et al., 1956; Kuffler, 1953). During active sensation, however, the sensors themselves move – scanning space to provide greater coverage of the outside world

[5]Corresponding author & Lead Contact: hadesnik@berkeley.edu.
[4]Equal contributors

Author Contributions

Conceptualization, S.R.P. and H.A.; Methodology, S.R.P., E.H.L., and H.A.; Investigation, S.R.P., E.H.L., G.I.T., and E.R.; Formal Analysis, S.R.P., E.H.L., and G.I.T.; Writing, S.R.P., E.H.L., and H.A.; Supervision, H.A.

(Kleinfeld et al., 2006). How neurons in the cortex encode scanned space, and whether integration across the sensor array is involved, is not known. Furthermore, sensor scanning has the potential to create its own spatial map in the cortex, not of the sensor array itself, but of the space swept out by the sensors. Such a map of scanned space could provide a basis for fine object localization and identification needed for behaviors such as prey capture, predator avoidance, and navigation.

The rodent whisker system is an advantageous system to address this question (Brecht, 2007; Feldmeyer et al., 2013; Petersen, 2007). On one hand, the topographic and discretized representation of the rodent's whiskers along the sensory hierarchy facilitates detailed analysis for how sensory neurons perform multi-whisker integration (Woolsey and Van der Loos, 1970). On the other, the stereotyped pattern of whisking during spatial exploration facilitates investigation into the sensorimotor processes underlying active sensation (Diamond et al., 2008; Hartmann, 2011). Decades of physiological analysis have quantified how spatial summation across the whisker array influences the cortical representation of touch (Armstrongjames et al., 1992; Boloori and Stanley, 2006; Brecht et al., 2003; Brecht and Sakmann, 2002; Brumberg et al., 1996, 1999; Chen-Bee et al., 2012; Ego-Stengel et al., 2005; Estebanez et al., 2012; Ghazanfar and Nicolelis, 1999; Goldreich et al., 1999; Higley and Contreras, 2003; Hirata and Castro-Alamancos, 2008; Kwegyir-Afful et al., 2005; Mirabella et al., 2001; Moore and Nelson, 1998; Moore et al., 1999; Petersen et al., 2001; Ramirez et al., 2014; Shimegi et al., 2000a; Zhu and Connors, 1999). Yet nearly all these investigations have utilized passive whisker stimulation, which can only probe receptive fields in discretized whisker space, and not in the continuous space scanned by the whiskers. An artificial whisking paradigm in anesthetized animals has allowed investigators to probe spatial coding during active touch, albeit in a reduced brain state (Brown and Waite, 1974; Castro-Alamancos and Bezdudnaya, 2015; Szwed et al., 2003; Wallach et al., 2016; Yu et al., 2015). These studies have revealed how spatial summation and the vibrissotopic map evolve across the sensory hierarchy or change dynamically with experience (Feldman and Brecht, 2005; Fox, 2002; Oberlaender et al., 2012).

Surprisingly, despite the well-ordered anatomical topography of the barrels in L4 (Woolsey and Van der Loos, 1970), two-photon imaging in layer 2/3 (L2/3) has revealed that on the cellular scale, the whisker map breaks down, exhibiting a salt and pepper tuning for whisker preference (Clancy et al., 2015) with some spatial correlation on the more global level (Sato et al., 2007). Similar receptive field studies in other rodent cortical areas, such as the auditory and visual cortices, have also found local breakdowns in maps of sensory space (Bandyopadhyay et al., 2010; Rothschild et al., 2010; Smith and Hausser, 2010), despite some evidence of an underlying organization (Ringach et al., 2016). Nonetheless, these works analyzed maps of a fixed sensor array and not of scanned space. It remains uncertain whether an orderly map of scanned space exists in the barrel cortex or elsewhere.

During active touch, barrel cortex neurons are often well tuned to the horizontal location of an object (Pluta et al., 2015; Yu et al., 2015). Multiple mechanisms potentially contribute to their tuning. These include selectivity for the phase (Curtis and Kleinfeld, 2009), deflection angle (Knutsen et al., 2008), inter-contact interval (Crochet et al., 2011), or contact forces (Bagdasarian et al., 2013; Yang and Hartmann, 2016) at the moment of touch. These

schemes can all operate at the single whisker level, and do not require multi-whisker integration, which is likely to occur in most natural contexts. Several studies have found that rodents perform better on whisker-guided behaviors when using multiple whiskers, suggesting that multi-whisker integration is critical for perceptual acuity (Knutsen et al., 2006; Krupa et al., 2001; O'Connor et al., 2010a). Although spatial summation is not required for spatial tuning *per se*, multi-whisker integration could powerfully transform the cortical representation of space. This might be particularly true during active sensing, where neighboring sensors probe overlapping regions of space. This raises the possibility that multi-whisker integration during active sensing might transform a discretized vibrissotopic map into a continuous map of scanned space that could be highly advantageous for object localization and discrimination.

Whether such a map exists in the barrel cortex, and, more specifically, how multi-whisker integration could shape its organization, is unknown. Most prior studies of the barrel cortex during active sensation have either been done in unrestrained animals, when controlling the stimulus is challenging, or in head-fixed mice where only a single whisker is left intact. One study in unrestrained animals quantified tactile responses before and after removing select whiskers surrounding the principal whisker (PW) column and found opposing effects in the cortex and the thalamus (Kelly et al., 1999). Yet in these freely behaving conditions, precise measurements of neuronal receptive fields could not be obtained.

We used two photon imaging and multi-electrode array physiology to address spatial summation and map organization in the somatosensory thalamocortical system. First, we tracked how spatial summation evolves across four stages of the sensory hierarchy, from the thalamus through three cortical layers. We found that neurons in the cortex, but not in the thalamus, exhibited an asymmetric, rostro-caudal gradient of summation over surround whiskers. Surround modulation not only had dramatic impacts on firing rates, but also generated a heterogeneous and substantial shift in the spatial preference of most neurons. On the population level, our data reveal a highly ordered and continuous map of scanned space in L2/3 of the barrel cortex. This map was nearly absent when only a single whisker was intact, indicating that summation over surrounding whiskers is critical to map organization. These data demonstrate that multi-whisker integration in the cortex organizes the spatial preference of neurons to create a continuous map of scanned space. Maps of scanned space may contribute to high fidelity encoding of the location and shape of objects during natural exploration.

Results

Quantifying spatial coding and summation during active sensation

To address how barrel cortex neurons encode scanned space and summate over whiskers in naturally whisking mice, we employed a head-fixed preparation in which mice ran on a free-spinning circular treadmill while we presented a vertical bar to the whiskers at fixed locations for 1.5 seconds (Fig. 1A). Mice were habituated to run for extended periods, a condition in which they move their whiskers in a highly rhythmic fashion (Pluta et al., 2015; Sofroniew et al., 2014) (Fig 1G). Under these conditions we could measure and quantify spatial representations with high precision. Neural activity was recorded with two-photon

calcium imaging in the upper cortical layers or multi-electrode arrays in the lower cortical layers and the ventro-posterior medial nucleus of the thalamus (VPM). Neural data was analyzed in the final 500 ms of stimulus presentation, during which neural activity and whisking kinematics had returned to a stable state after abrupt positioning of the stimulus bar (Fig. S1). Experimental trials were selected based on the velocity and consistency of treadmill running to minimize variation in whisking behavior (Fig. S1E, and see Methods). This strict sampling of running behavior ensured consistent, repetitive touches with the stimulus throughout the object presentation period (Fig. S1F). Prior to each experiment, we first identified the location of the C2 whisker's representation in each mouse using intrinsic optical imaging. In both imaging and electrophysiology experiments, we found neurons across all layers of the barrel cortex whose tactile-evoked responses were tuned to the horizontal location of the vertical pole (Fig 1B–D). By labeling a single 'principal whisker' (PW) in a subset of mice with reflective paint we could track this whisker reliably in the presence of all other whiskers (Fig. 1E–H, Fig. S1). Using high-speed whisker tracking we found that across the full 'whisking field' the PW made rhythmic contact with the stimulus bar throughout the stimulus period at central but not lateral locations, where only adjacent whiskers (AWs) contacted the bar, defining a principal whisker contact zone (PWCZ) and an adjacent whisker contact zone (AWCZ, Fig. 1E,F).

To explore spatial summation during active sensation, we sought to quantify the contribution of the PW and the AWs to each neuron's spatial representation. We reasoned that we could measure this by comparing a neuron's spatial tuning function before and after acutely trimming off all the surround whiskers. The difference in these two measurements would reveal the parallel contributions of the AWs and PW to each neuron's spatial receptive field. Towards this aim, we collected spatial tuning curves both before and after trimming all but the principal whisker in a single experimental session (< 1 hour), so that after trimming, only the PW could contact the stimulus bar. Importantly, whisker trimming on such an acute time-scale is much shorter than required for the induction of sensory-deprivation induced plasticity (Bender et al., 2006; Glazewski and Fox, 1996; Wen et al., 2013). The dataset consisted of 1016 neurons in L4 (340±120 ROIs/mouse; 3 mice), 2572 neurons in L2/3 (640±120 ROIs/mouse; 4 mice), 172 regular spiking (RS) units in L5 (10±2 units/mouse; 16 mice), and 90 units in VPM (11±2/mouse; 8 mice). Since acute whisker trimming might alter an animal's pattern of whisking during active sensation, in a subset of mice we tracked the PW both before and after surround whisker trimming and found that trimming did not significantly alter the kinematics of the animals' whisking patterns, except for a minute difference in amplitude (Fig. S1, mean ± s.e.m: 0.90 ± 0.20 degrees, far smaller than the 10–15 degrees between presented stimuli). This indicates that any changes we observed in neuronal response functions were due to changes in neural computation and not to changes in whisking behavior.

Spatial summation in L4

First we addressed spatial coding and summation in excitatory neurons in L4 of the barrel cortex. To record from a large population of L4 excitatory neurons across the spatial map in S1 we expressed GCaMP6s (Chen et al., 2013) in excitatory neurons in L4 using a Cre-dependent AAV and a L4-specific Cre line (Madisen et al., 2010; Pluta et al., 2015) (Fig.

2A). Prior to whisker trimming we observed contact-evoked responses across the entire imaging field. Following removal of the surround whiskers, sensory evoked responses were essentially abolished outside of the PW 'column' (68 ± 9% decrease in number of significantly driven units, n = 3 mice, for column identification see Methods and Fig. S2), demonstrating that the PW preferentially drives touch responses within its anatomically aligned column, consistent with prior observations under both passive and active conditions (Goldreich et al., 1999; Hires et al., 2015). Strikingly, in the rostral position of the PWCZ the majority (56 ± 8%, n = 3 mice) of L4 neurons within the PW column exhibited significant enhancements in their contact-evoked activity following surround whisker trimming (4.0 ± 1.3 fold increase in population mean, n = 231, Wilcoxon sign rank, $p < 0.001$, Fig. 2B–E). We computed a 'trimming index' as a metric for how surround whiskers influenced the evoked firing rate of each given neuron, defined as the difference over the sum of evoked activity between pre and post-trimming conditions. In the rostral PWCZ position, nearly all neurons had a positive trimming index, indicating pronounced disinhibition following surround whisker trimming (trimming index = 0.33 ± 0.03, n = 231, $p < 0.001$, Wilcoxon sign rank, Fig. 2F). In contrast, in the caudal PWCZ position, most neurons showed a reduction in tactile evoked response (0.8 ± 0.1 fold decrease in population mean, trimming index = −0.30 ± 0.03, n = 231, $p < 0.001$, Wilcoxon sign rank, Fig. 2F). These data indicate that surround input from more caudal whiskers provides facilitation, whereas input from the more rostral whiskers primarily provides suppression. To address how surround whisker input influences spatial coding, we computed an index of spatial preference (the center of mass of the spatial tuning curve in the PWCZ). We found that for nearly all L4 neurons that exhibited spatial tuning (1-way ANOVA), spatial preference shifted forwards (1.77 ± 0.09 mm mean shift, n = 139, $p < 0.001$, t-test, Fig. 2G).

Spatial summation in cortical projection layers

Next we addressed spatial coding and summation in L2/3 and L5, the two major output layers of the barrel cortex. In L2/3 we used two-photon imaging (110–195 microns deep) to sample a large number of L2/3 neurons across the spatial map in S1. In L5 we employed laminar multi-channel electrodes that spanned the complete depth of L5. The laminar position of the electrode in each experiment was confirmed with a combination of depth readings off a precise micromanipulator, current source density analysis of the touch-induced local field potential (LFP), and post-hoc histology of the electrode track (Fig. S2). Prior to any trimming, we observed that L2/3 and L5 neurons in the PW column very often exhibited substantial evoked activity in the AWCZ, the region where the PW makes no contact (Fig S2), consistent with prior imaging studies showing that a single whisker could evoke broad activity across multiple barrel columns in L2/3 (Clancy et al., 2015; Peron et al., 2015). This is in contrast to neurons in L4 and in VPM which responded more specifically (but not exclusively) to stimuli within the PWCZ (see Fig. S2). This suggests that surround whisker input in L2/3 and L5 might be particularly important for spatial representations in these cortical projection layers.

To address this hypothesis, we recorded tactile evoked responses in both layers prior and subsequent to trimming all but a single whisker, as above. L2/3 exhibited suppression in the anterior PWCZ, but nearly exclusive facilitation in the caudal PWCZ (rostral position

trimming index = 0.14 ± 0.02, n = 631, p < 0.001, Wilcoxon sign rank; caudal position trimming index = −0.37 ± 0.02, n = 631, p < 0.001, Wilcoxon sign rank, Fig. 3B–F). As a consequence, surround input altered the spatial preference of L2/3 neurons, but did so somewhat more heterogeneously than L4, with most neurons shifting rostrally, but some shifting caudally in their preference (1.42 ± 0.07 mm mean shift, n = 413, p < 0.001, Wilcoxon sign rank, Fig. 3G). In L5, similar to L2/3, the predominant impact of surround input was to facilitate responses at the caudal PWCZ position (37 ± 7% mean decrease in spike rate, mean trimming index = −0.29 ± 0.06, n = 48, p < 0.001, Wilcoxon sign rank, Fig. 4A–D), which likewise had the net effect of altering spatial preference in most neurons (0.6 ± 0.2 mm mean shift forward, n = 39, p = 0.001, Wilcoxon sign rank, Fig. 4E).

As a control for these changes, we performed a separate set of experiments where we sham trimmed the whiskers (total experimental time equal to trimming experiments), and observed no significant effects on the population, demonstrating that the neural responses were stable over the recording session (Fig. S3). In addition, to assess the stability of spatial preference in each neuron in the trimming datasets, we analyzed the first and second halves of the control and trimmed whisker trials separately. We found that the spatial preference of neurons within each condition were stationary over time (Fig. S3), further indicating that slow changes in neuronal response properties independent of surround whisker trimming cannot explain our results. To determine how spatial preference evolves over the time course of object presentation, we analyzed each neuron's activity during eleven different time windows during object presentation. We found that the trimming-induced forward shift in spatial preference plateaued for analysis periods starting more than 600 ms after object presentation (Fig. S4). This result agrees with our behavioral analysis of whisking set-point, which stabilized approximately 600 ms after object presentation (Fig. S1C), also emphasizing the importance of analyzing the neural data in a time window of high behavioral consistency. It should also be noted that the temporal resolution of GCaMP6s as a reporter of neural activity is substantially lower than that of electrophysiology. Nevertheless, GCaMP6s activity during our analysis period displayed temporal dynamics not too dissimilar from electrophysiology (Fig. S4 E&F).

Spatial summation in the somatosensory thalamus

The data described above demonstrate that surround whisker input powerfully influences how cortical neurons represent scanned space. Which of these surround effects emerge in the cortex, and which are inherited upstream via the thalamus? Whisker pathways converge even at the brainstem level, and can contribute to multi-whisker receptive fields in the thalamus (Timofeeva et al., 2004). To answer this question, we recorded from thalamic neurons in the ventro-posterior medial nucleus (VPM, dorsomedial portion) and compared the impact of surround whisker input on VPM neurons to our observations in cortical neurons. We found that thalamic neurons showed robust spatial tuning like their cortical counterparts (fraction of neurons tuned, VPM: 83%, L4: 86%, L2/3: 89%, L5: 67%, 1-way ANOVA), demonstrating that tuning, *per se*, is likely to be generated sub-cortically, perhaps as early as the primary mechanoreceptors, according to previous reports (Szwed et al., 2003; Yu et al., 2015) (Fig. 5A–C). Nevertheless, trimming the surround whiskers demonstrated that surround input modified thalamic responses, but weakly compared to L4 (Fig. 5D–E). A

minority of VPM neurons exhibited a significant change in their evoked activity across the center of their spatial receptive field (within the 'PWCZ', Fig. 5D). As a population, VPM neurons displayed a reduction in their evoked firing rate at the rostral PWCZ position (trimming index = −0.13 ± 0.06, p = 0.047, n = 54, paired t-test, Fig. 5E). This distinctly contrasts to the robust enhancement we observed in L4 neurons at the rostral PWCZ position. Furthermore, unlike for cortical neurons, surround input did not change the spatial preference of VPM neurons (0.16 ± 0.14mm mean shift, n = 51, p = 0.23, t-test, Fig. 5F). These results imply that surround modulation of the spatial preference of cortical neurons emerges primarily in the cortex.

As a whole, the data above demonstrate that surround input uniquely transforms the cortical representation of space. Conversely, we sought to determine the importance of principal whisker (PW) input to spatial tuning in an output layer of the cortex, L5. Towards this end, in a separate set of mice, we measured spatial tuning functions before and after trimming off only the PW, leaving all the surround whiskers intact (Fig. S5). Following removal of the PW, we observed a pronounced reduction in the evoked firing rates of neurons that were facilitated by touch, consistent with the expected function of the principal whisker (−28 ± 5% change, trimming index: −0.20 ± 0.03, Fig. S5a, n = 36, p < 0.001, paired t-test). Even though almost all (95%) L5 units retained significant touch-evoked firing after removal of their PW, they exhibited no change in spatial preference (Fig. S5C, n = 20, p = 0.53, Wilcoxon sign rank), in notable contrast to the effect of removing surround whiskers. However, the spatial selectivity of the population was significantly reduced, typified by flatter tuning curves (n = 50, p = 0.003, Wilcoxon sign rank, Fig. S5D). These data indicate that the PW is the primary, but not sole, contributor to the amplitude of a given neuron's tactile response, while surround whiskers potently influence its spatial preference.

Surround input organizes a map of scanned space in the barrel cortex

The data above indicate that surround whisker input powerfully influences how individual neurons in the barrel cortex encode scanned space. How might spatial coding be organized on the more global level? On one hand, the spatial preference of nearby neurons might show little correlation, similar to the salt and pepper distribution of orientation tuning in rodent visual cortex (Ohki et al., 2005). Alternatively, the spatial preference of neurons might gradually shift across the rostro-caudal axis of cortex, constituting a continuous map of scanned space. To address this question in L2/3, we plotted spatial preference for each neuron across the entire field of view (1.06 ± 0.30 mm^2), encompassing the region above several adjacent barrels (Fig. S6). Strikingly, we observed a topographic representation in the positional preference of neurons across the rostro-caudal axis of stimulus space, arranged approximately across the row axis of the barrel cortex (Fig. 6A, see Methods and Fig. S6 for a description of how the map axis was determined). The spatial resolution of the aggregated maps was 6.7 μm of physical space per micron of cortical tissue, as quantified by the slope of the linear regression of spatial preferences across all mice (Fig. 6D).

Since we did not observe clear discretization in any of the individual maps (see Fig. S7), it is possible that summation over surround whiskers help generate this continuous map. To test this idea, we asked how the spatial map changed following removal of all but one whisker.

While many neurons across the entire field of view retained significantly evoked responses and spatial tuning, the spatial map all but disappeared (Fig. 6B, Fig. S7). We quantified this change in several ways. First we compared the correlation of neurons' spatial preference across the axis of best fit before and after trimming (see Methods). Before trimming, the spatial preference of the imaged neurons exhibited a clear correlation along the rostro-caudal axis (Pearson's $R = 0.70$, $p < 0.001$), implying the presence of a map; however, after trimming, this correlation disappeared (Pearson's $R = 0.00$, $p = 0.9$, Fig. 6D–E). This relationship held true both across the entire field of view and within a restricted zone that retained strong activity following trimming (Pearson's R pre-trim = 0.48, $p < 0.001$, vs. Pearson's R post-trim = 0.08, $p = 0.063$), most likely corresponding to the region directly above the spared L4 barrel (486 ± 70 microns along axis of best fit, n = 4 mice). Second, we computed correlations between the spatial preferences of all pairs of neurons within a given map as a function of cortical distance along the axis of best fit. For a map to exist, nearby neurons should display similar spatial preferences, while distant neurons should diverge. Consistent with this notion, before trimming, an analysis of pairwise correlations show that nearby neurons have much greater similarity in spatial preference than distant neurons (Fig. 6F). However, after trimming to a single whisker, the relationship between pair-wise cortical distance and spatial preference similarity dramatically decreased (Fig. 6F). As a third means to quantify this map, we constructed cumulative distribution functions of spatial preference along the axis of best fit before and after trimming. With surround input intact, there was a gradual and systematic tiling of spatial preference along the entire axis of cortical space ($p < 0.001$, ANOVA, n = 1486, Fig. 6G). Following trimming to the C2 whisker, these spatial preference distributions coalesced (Fig. 6H), due to an increasingly greater forward shift in caudal neurons (Fig. 6I), demonstrating that multi-whisker integration is critical for an organized map of the scanned region. The apparent disorganization of the map was not simply due to noisier responses in the cortex after trimming, since our analysis is restricted to neurons significantly tuned for space and significantly driven by the stimuli. Nor is it due to analyzing different total numbers of responsive and tuned neurons between the two conditions, since the results held true even when we restricted our analysis to the population of neurons that were significantly tuned both before and after trimming (Fig. S8). Lastly, we addressed whether behavioral variation, such as minute trial-to-trial differences in whisker set-point, could have affected the smoothness (Pearson's R) of the sensory map in L2/3. However, in our L2/3 dataset, the faster the mouse ran on the treadmill (the narrower the range of whisker set-points, Fig. S1), the smoother the map became (Fig. S8). Therefore, behavioral variation is in fact detrimental to map smoothness.

Finally, we probed this spatial map electrophysiologically using multi-shank laminar electrodes (Fig. 7A, B). We inserted three 8-electrode shanks across the C-row axis of the barrel cortex (identified with intrinsic optical imaging and electrophysiologically verified, Fig. S2) and measured spatial tuning functions of cortical units across 3 barrel columns both before and after trimming to the C2 whisker (Fig. 7C, D). Across the electrode shanks, the rostro-caudal distributions of spatial preference could be quantified by plotting cumulative distribution functions. Before trimming, neurons in different cortical columns had significantly different spatial preferences that corresponded to their relative location in the cortex ($p < 0.001$, ANOVA, n = 70, Fig. 7C, E). After trimming, the spatial preference of the

neurons that retained significant tuning coalesced onto a narrow region of space ($p = 0.32$, ANOVA, $n = 45$, Fig. 7D, F). Furthermore, the magnitude of the change in spatial preference varied with cortical location; neurons in the caudal cortical column shifted further forward than neurons in the rostral column ($p = 0.03$, ANOVA, $n = 31$). These results are not simply due to inferior measurements of spatial preference caused by a uniform reduction in response strength, because the spatial selectivity of neurons outside of the spared column did not systematically decrease after trimming ($p = 0.73$, $n = 24$, Wilcoxon sign rank). Although these electrophysiological recordings cannot reveal the same degree of continuity we observed with two photon imaging, they nevertheless further support the notion that surround whisker input distributes the spatial preference of neurons to generate a map of scanned space in the barrel cortex. Lastly, we asked if the map was centered on the head, rather than on the set point of the whisking envelope. If so, the spatial preference of neurons should stay the same, despite a shift in whisker set-point. However, we observed that spatial preference follows the set-point of whisking, implying that the map is not head-centered (Fig. S9).

Discussion

This study examines how neurons across four sequential stages of the thalamocortical system integrate across a sensor array during active sensation to encode the space scanned by the sensors, in this case, the rodent's whiskers. While many previous studies have addressed spatial summation in anesthetized, paralyzed, or fixating animals, how summation influences sensory coding when the sensors are actively and volitionally moving has remained largely unexplored. Several previous studies have compared neural responses between active and passive conditions and reported significant differences, including reduced response amplitudes and more restricted spatial or temporal spread of activity (Fanselow and Nicolelis, 1999; Ferezou et al., 2007; Hentschke et al., 2006; Lee et al., 2008). Yet spatial summation, *per se*, has not been rigorously characterized in awake, volitionally whisking mice. In this study, we found that surround whisker input potently transformed barrel cortex neurons' spatial tuning, strongly impacting firing rates, and shifting their spatial preference. In L2/3, these shifts acted to organize a sensory map of scanned space. Such a map – referenced not to the sensors, but instead to the space probed by the moving sensor array, has not been previously demonstrated in any sensory system to our knowledge. Although the whisker system bears many unique qualities that distinguish it from other sensory systems, this spatial map of scanned space in the barrel cortex raises the possibility that similar maps might exist in other cortical areas in rodents, and in other mammalian species. Primates move their hands across surfaces to localize and identify objects (Chapman and Ageranioti-Belanger, 1991), similar to how rodents use their whiskers, and a continuous map of scanned space in the primate somatosensory cortex might also exist.

The map we observed was not an ego-centric map – i.e., a head-centered map – but rather a map centered on the set-point of the scanned region (Fig. S9). Nonetheless, a map of scanned space, as was observed here, may contribute to the generation of an egocentric (head-centered) map of space downstream that is independent of the scanned region (or 'field of view'). Based on prior evidence in non-human primates, the posterior parietal

cortex is a brain area that may be involved in this transformation (Andersen et al., 1985), but likely builds on cues present even at the mechanoreceptors themselves (Yang and Hartmann, 2016).

How might a map of scanned space be generated? First, it is important to note that while the map depends on summation over multiple whiskers, spatial tuning for individual cortical neurons persists even with only a single whisker intact. This is largely consistent with prior reports that horizontal location can be computed by cortical neurons even with information from a single whisker (Curtis and Kleinfeld, 2009; O'Connor et al., 2010b), or even by neurons at very early stages of the somatosensory system (Szwed et al., 2003; Yu et al., 2015), a fact consistent with the strong tuning we observed in thalamic neurons. Thus horizontal tuning *per se* does not appear to depend on cortical computation. Instead, we propose that summation over the underlying whisker map, specifically in the cortex, is what helps create the map of scanned space. This computation might be analogous to local smoothing, and could be implemented by the broad dendritic trees and horizontal projections of L2/3 pyramidal neurons that cross cortical column boundaries, as well as the divergence of ascending L4 axons (Bender et al., 2003). Nevertheless, many other possibilities exist, including computations involving efferent or re-afferent signals of whisker motion. While future experiments can address the underlying mechanisms that generate the map of scanned space in L2/3, we propose that the role of surround input in the cortex is not to generate spatial coding *de novo*, but rather to act on the global level to organize spatial preference across the horizontal axis of the cortex in such a way so as to generate a continuous map of space. Whether other maps that exist in the barrel cortex, such as for contact angle or for correlation selectivity, contribute to the generation of this spatial map, remains to be seen (Andermann and Moore, 2006; Estebanez et al., 2016; Kremer et al., 2011; Peron et al., 2015).

In this study, owing to the highly stereotyped pattern of whisking that mice exhibit during head-fixed locomotion, we were also able to reliably quantify single neuron’s spatial tuning curves during active sensation. Although this preparation resembles in some respects anesthetized conditions where the whiskers are made to move artificially by electrical stimulation of the facial motor nerves (Brown and Waite, 1974; Castro-Alamancos and Bezdudnaya, 2015; Szwed et al., 2003), all of our data were collected in the awake, alert state. Since several studies have highlighted how brain state and the level of alertness can dramatically influence sensory processing and the firing of specific cortical subtypes (Adesnik et al., 2012; Castro-Alamancos, 2004a, b; Castro-Alamancos and Oldford, 2002; Greenberg et al., 2008; Lee et al., 2013; Niell and Stryker, 2010; Poulet and Petersen, 2008; Reimer et al., 2014; Vinck et al., 2015), we consider it essential that we performed all of our experiments in the awake state while mice ran and whisked of their own volition.

The second key finding of this study with respect to spatial summation is the presence of an asymmetric rostro-caudal gradient of response modulation that emerges in the cortex. This modulation is most pronounced in L4, where contact with anterior whiskers powerfully suppresses responses to the PW, while contact with more posterior whiskers generate substantial facilitation. This effect is very likely to be related to the well-known impact of the temporal sequence of whisker-object contacts revealed in anesthetized recordings

(Civillico and Contreras, 2006; Drew and Feldman, 2007; Higley and Contreras, 2003; Shimegi et al., 2000a, b). What is the utility of such across-whisker modulation? One possibility is that the combined action of anterior suppression and posterior facilitation strongly enhances spatiotemporal contrast in the population response in L4 during whisker contact. In other words, as an animal sweeps its whiskers forwards into an object, the largest neural responses will be in the barrel representing the first whisker to contact the stimulus, both because it gets no suppression from any anterior whisker and because it gets facilitation from the more posterior whisker that contacts the object second. However, at the same time, the L4 barrel representing the second whisker to touch will be suppressed by touch with the first whisker. The net effect of this scheme is to generate a high spatial gradient of evoked responses in L4 barrels that could sharpen the population representation of touch in the barrel cortex (Brumberg et al., 1996; Drew and Feldman, 2007). This contrast-enhancing, asymmetric integration appears to be involved in generating the continuous map of scanned space we observed in L2/3, although it could be important on its own for other spatial computations. Additional factors unrelated to timing, such as asymmetry in forces on the PW across different object positions, likely shape the properties of surround integration.

Taken together, the results of this study reveal fundamental modes of cortical computation during active sensation, and shed light on key underlying neural mechanisms. Previous studies, primarily in anesthetized or sedated animals, have highlighted how summation across whiskers depends critically on the timing and spatial patterns of surround whisker stimulation (Brumberg et al., 1996; Shimegi et al., 2000a). In at least two studies, coordinated waves of surround input, mimicking that which occurs naturally, can profoundly alter the response properties of cortical neurons (Drew and Feldman, 2007; Jacob et al., 2008). In this study, since the animals whisked freely, the timing and pattern were not under experimental control, but our results are nevertheless consistent with prior experiments under anesthesia. A previous study, in anesthetized animals, demonstrated that the degree of correlated whisker movement across the array could profoundly influence single unit responses – with some units enhanced and other suppressed by global correlations (Estebanez et al., 2012). Furthermore, recent work showed that the enhanced neurons in L2/3 are clustered above the edges of the L4 barrels (Estebanez et al., 2016). In our study, since the mice naturally whisked in a coherent fashion at a vertical bar, the stimulus we used is likely to be more similar to the global correlation condition. In any condition, the precise spatiotemporal pattern of multi-whisker touch likely has a profound influence on sensory integration. Similar to previous studies that investigated active sensation with a single whisker (Ferezou et al., 2007; Hentschke et al., 2006; Lee et al., 2008), our results have the advantage that they are drawn from volitionally whisking mice, and thus within the ethologically relevant range of multi-whisker contact patterns. However, this naturalistic approach prevented us from identifying the precise moments of multi-whisker touch, thereby obscuring the effects of multi-whisker integration on the fine temporal structure of spiking. Future studies, using technological advances that permit the imaging and quantification of multi-whisker contacts during exploration of objects with complex surface geometry (Hobbs et al., 2016), in combination with the physiological approaches here, could address how a spatial map in S1 facilitates the encoding of higher order stimulus features. Furthermore, processing stages downstream of S1 could integrate topographic information of scanned

space with sensorimotor signals conveying whisking set point to construct an egocentric map of space.

STAR Methods

Contact for Reagent and Resource Sharing

Further information and requests for resources and reagents should be directed to and will be fulfilled by the Lead Contact, Hillel Adesnik (hadesnikberkeley.edu).

Experimental Model and Subject Details

Wild-type adult ICR white (Charles River) mice between 6 and 10 weeks of age and of either gender were used for all experiments, except for those involving imaging cortical layer 4, for which the scnn1-tg3-Cre line (JAX), outcrossed to the ICR line for several generations, was used. All procedures were approved by the Animal Care and Use Committee of UC Berkeley. Both female and male animals were used and maintained on a 12:12 reversed light:dark cycle. For Supplemental figure 6, we used a Thy1-GCaMP6s (4.3) mouse.

Methods Details

Preparation for *in vivo* electrophysiology—Anesthesia was induced with 5% isoflurane and then maintained at 1 – 3% during surgery. Respiratory rate and response to toe/tail pinching was monitored throughout surgery to ensure adequate anesthetic depth. 0.05 mg/kg of buprenorphine was administered for post-operative analgesia. After disinfecting the scalp with 70% alcohol and 5% iodine, the skin and fascia above the sensory cortices were removed with surgical instruments. Following application of Vetbond (3M) to the skull surface and wound margins, a custom stainless steel headplate was fixed to the skull with dental cement (Metabond). Two days after surgery, mice were habituated over increasing durations for 4 – 8 days to head-fixation on a free-spinning circular treadmill, until they freely ran at a fast and steady pace (>35 cm/s). Intrinsic optical imaging was performed to localize one or two barrel columns of interest (C1 – C3). In preparation for electrophysiology, mice were briefly (10 – 15 minutes) anesthetized with isoflurane, the skull over S1 was thinned with a dental drill (Foredom), and a small (<200 μm for a single shank) craniotomy was made with a 27 gauge needle. For mutli-shank experiments a long, thin craniotomy was opened over S1 in a similar fashion. The small size of the craniotomy minimized motion of the brain during electrode penetration and animal movement. For recordings from the cortex, a 16 or 32-channel linear silicon probe (NeuroNexus) was guided into the brain using a micromanipulator (Sutter Instruments) and a stereomicroscope (Leica) to the desired barrel column (C1 – C3) by aligning the intrinsic optical signal (Fig. S2) with superficial blood vessels. For multi-shank experiments, a Neuronexus Buzsak32 probe was used. The principal whisker was verified electrophysiologically by deflecting individual whiskers and listening to multiunit activity (MUA). There was an audibly clear difference in MUA between principal and surround whisker contact. For recordings of the thalamus, a 16-channel linear silicon probe (NeuroNexus) was guided into the brain at 1600 μm posterior and 2000 μm lateral from bregma. The electrode was lowered until strong whisker responses were detected, usually around 2700–2800 μm, indicating the border of the

ventro-posterior medial nucleus. The electrode was lowered further until it reached a barreloid corresponding to C2 or B2, where that whisker caused the strongest response from deflection. In all cases, electrical contacts on the probe spanned the C1 – C3 or B1 – B3 barreloids, as verified by electrophysiology.

Preparation for *in vivo* two photon imaging—The surgery was as described above, but with the following modifications for transcranial imaging through a glass window. 2 mg/kg of dexamethasone were administered as an anti-inflammatory. A 3 mm diameter craniotomy over the left primary somatosensory cortex was drilled, and a Nanoinject II nanoliter injector was used to inject 18.4 nL of AAV-GCaMP6s at ten to twenty sites within the craniotomy at an overall rate of 0.5 nL/s. AAV9-synapsin-GCaMP6s (UPenn Vector Core) was injected into wildtype ICR mice (Charles River) for L2/3 datasets, and AAV9-flexed-CAG-GCaMP6s (UPenn Vector Core) was injected into scnn1-tg3-Cre mice (JAX) for L4 datasets. After viral injection a window plug consisting of two 3mm diameter coverslips glued to the bottom of a single 5mm diameter coverslip using Norland Optial Adhesive #71 was placed over the craniotomy and sealed permanently using Orthojet. Mice were head-fixed on a freely spinning running wheel under a Nixon 16×-magnification water immersion objective and imaged with a Neurolabware two-photon resonant scanning microscope within a light tight box. Image acquisition was at 15.45 Hz with fields of view (FoVs) ranging from 600 μm by 650 μm to 1.25 mm by 1.15 mm. To obtain large fields of view in all cases, in some experiments four adjacent FoVs were imaged sequentially. Wide-field reflectance imaging with a white LED was used to illuminate the vasculature and center the FoV on the region the intrinsic signal identified as corresponding to the C2 barrel. For L2/3 imaging, imaging depth was 100 – 300 μm, and for L4 imaging, depth was 400 – 500 μm deep.

Tactile Stimulus presentation—During continuous two-photon imaging or electrophysiological recording, a modified 0.7mm Hex key (McMaster-Carr) was presented vertically at 8 locations along an axis perpendicular to whisking motion and ~1 cm away from the mouse's face. The pole was presented to the whiskers for 1.5 seconds during each trial using a stepper motor (Oriental Motor) to quickly move the pole in, hold the pole stationary for the entire stimulus period, and then move it back out. There was an interval of 3 – 4.5 seconds between trials for imaging to allow the evoked calcium response to return to baseline. At the beginning of each inter-trial interval the stepper motor and pole were translated to the next trial's horizontal position using a motorized linear stage (Zaber). Stimuli were randomized in batches such that no stimulus was presented more than twice in a row. After >15 repetitions of the stimulus batches, data collection was paused and all but the principal whisker (always C2 for imaging experiments) were trimmed such that only the remaining whisker could contact the vertical pole stimulus at any position. Data collection immediately recommenced and at least 16 new batches of stimuli were presented. After conclusion of the experiment, the vertical pole was presented at each of the stimulus positions, and the PWCZ positions were identified by high speed camera acquisition or by visual inspection using stereomicroscope. This was verified post-hoc by determining which stimulus positions evoked significant activity throughout the object presentation period after trimming the surround whiskers.

Two photon imaging analysis—Raw two photon movies were first corrected for brain motion using Scanbox's fourier transform-based sbxalign script, written in MATLAB, to correct for the 2D translation of individual frames. The mean of each motion-corrected video was used to translate and register the before and after trimming datasets to within a single pixel of each other. Regions of interest (ROIs) encompassing neurons were identified in a semi-automated manner using Scanbox's sbxsegmentflood (MATLAB, Mathworks) which computes and thresholds the pixel-wise cross-correlation for all pixels within a 60 by 60 pixel window. If an ROI only appeared in one of the datasets via the semi-automated method, then the ROI was copied over to its relative location in the dataset in which it was not identified. The ROI's signal (R_i) was taken as the mean value across all pixels within and unique to that ROI (Fig. S2). This signal is assumed to be a mixture of the cell's actual fluorescence signal and a contaminating neuropil signal resulting from scattering producing off-target excitation, high illumination powers producing out of focus fluorescence, or unresolvable neurites passing through the microscope's point spread function. The neuropil signal (N_i) for each ROI was computed by averaging over an annulus of pixels surrounding the ROI but excluded pixels assigned to other ROIs as well as a smaller annulus of pixels that acted as a buffer in case any motion artifact was not perfectly accounted for (Fig. S2). This buffer annulus existed for all ROIs and was excluded from any neuropil calculation. As a result the max diameter of the neuropil annulus varied per ROI in order to ensure a similar number of usable pixels to average over. Each neuron's true fluorescence signal (F_i) was computed per ROI by the following equation:

$$F_i(t)=R_i(t) - k_i * N_i(t)$$

The amount of contamination (k_i) was assumed to be constant per ROI, but vary between ROIs as a result of local differences in expression and scattering. Each k_i was defined by assuming that the neuron's true fluorescence signal (F_i) can never be negative (i.e. $k_i * N_i(t) \leq R_i(t)$), and that there must be a maximal bound for contamination. The contamination coefficient per neuron was defined as follows:

$$k_i=\min\left(\frac{R_i(t)}{N_i(t)}\right); \text{if } k_i>.65, k_i=.65$$

The true signal was then converted into a trial-wise change in fluorescence ($\frac{f(t) - f_0}{f_0}$ or df/f) to capture the stimulus-evoked changes in neural activity while compensating for any fluctuations in baseline fluorescence. The baseline fluorescence (f_0) for a trial was taken to be the mean fluorescence over the one second prior to stimulation.

High-Speed Whisker Tracking—In a subset of experiments the whiskers were tracked at high speed (~500 frames per second). Previous data, confirmed here (Fig. S1), indicate a tight correlation between run-speed of the mouse and whisker set-point, which plateaus above 35 cm/s (Sofroniew et al., 2014). A high-speed camera (Basler, acA2000-340kc) was placed below the running wheel; the principal whisker was imaged from below using a mirror angled at 45 degrees. The base of the PW was painted with a thin layer of Titanium

White (Liquitex) paint and illuminated from below using a bright red LED, providing contrast from the other whiskers. High-speed videos were acquired at 500 fps with a 100 μs exposure and were synchronized with neural data acquisition via external triggers. Videos were processed in MATLAB using custom tracking software. An ROI was placed over the sector that the painted whisker swept out, cropping out other reflective surfaces (e.g. mouse's nose) that would otherwise interfere with tracking. All frames were luminance-thresholded to create a binary image, and the center of the painted region was calculated; the angle between the center of the painted region and a user defined position on the face was calculated for all frames. Angle traces were created from these measurements to calculate the whisker kinematic features in Figure S1: set-point (median angle of envelope), amplitude (half-width of envelope), speed (distance/time), and frequency (cycles/second). The image of the PWCZ and the AWCZ in Figure 1 was created from tracking a mouse with a single row of whiskers illuminated from the top. The whisker traces were manually traced for display purposes only. It was not possible to detect contacts between the painted whisker and the stimulus bar, since only the base of the whisker was painted to avoid adding substantial weight to this whisker or altering its curvature.

Spike Sorting—16–32 channels of electrodes were amplified (AM Systems), filtered (0.1–5 kHz) and digitized at 30 kHz (National Instruments) using custom acquisition software (MATLAB, Mathworks). Spike detection was performed using the UltraMegaSort2000 package in MATLAB (Hill et al., 2011) (Mathworks). After detection, spikes were automatically sorted into clusters of units. Units were then further sorted manually to meet inclusion criteria and prevent pseudo-replication. Quality metrics included analysis of spike amplitude, spike rate, auto- and cross-correlation, inter-spike interval, outlier removal, distance from threshold, and cortical depth of largest waveform. With the exception of a small subset of fast-spiking or bursting units, included units had no more 1% of their individual waveforms violating a refractory period of 2.5 ms. The surround whisker trimming data was collected from 8 mice for the L5 RS population and 8 mice for the thalamus population. The principal whisker trimming data was collected from 8 separate mice.

Spike Waveform classification—Fast-spiking units were separated from regular spiking units using a k-means cluster analysis of two waveform components. One component was the normalized difference between the two positive-going peaks. The other component was the trough-to-peak latency of the large negative-going deflection. Fast-spiking units were categorized by a larger 2nd positive-going peak (positive difference), and a short (less than 0.33ms) trough-to-peak latency, following previously established approaches. Units on the border between the classification as FS or RS was excluded from analysis. FS neurons were excluded from the paper.

Trial inclusion criteria and layer boundaries—In sorted units, firing rates were computed by counting spikes in the final 500 ms of stimulus presentation. This window was chosen because within 1000 ms of the bar entering the whisker field, neuronal firing rates and behavior reached steady-state. Trials containing stimulation periods where the animal’s mean run speed during the stimulus period dropped below 1.3 standard deviations of it

population mean were excluded, to ensure consistency in whisking behavior across trials. In addition, trials where the standard deviation of an animal's run speed was more than 0.8 standard deviations from the population mean were excluded. Trials where the animal was not moving, thresholded by the animal's run speed being below 3 cm/s, were completely excluded from analysis. The depth of each unit was assigned based on the calculated depth of the electrode on the linear array that exhibited its largest waveform. Layer boundaries were confirmed post-hoc using current source density analysis (CSD, Fig. S2) and labeling of the electrode track with a dye. CSDs were calculated from the trial-averaged local field potential (0.5 – 300 Hz) measured at each electrode contact, as previously published. We estimated the layer 4/5 boundary as the base of the current sink corresponding to layer 4.

Analytical Metrics—A *Trimming Index* for each condition was computed as the difference between the mean evoked firing rates during post-trimming (T) and control (C) conditions, divided by the sum of their mean evoked firing rates:

$$\text{Trimming Index} = \frac{T - C}{T + C}$$

The *Spatial Preference* of a neuron was determined by calculating the center of mass (CM) on the absolute value of its spatial tuning curves. FR, the mean evoked firing rate (or delta F) at position, P, at stimulus locations 1 through n:

$$\text{Spatial Preference (CM)} = \frac{FR_1 * P_1 + FR_2 * P_2 + \ldots + FR_n * P_n}{FR_1 + FR_2 + \ldots + FR_n}$$

Statistically significant changes in spatial preference at the level of single units was computed using a standard permutation test. For each unit, a null distribution of change in spatial preference was created by randomly sampling values among both conditions 5000 times. Significance ($p < 0.05$) was observed if the experimental effect was beyond the 97.5 percentile or below the 2.5 percentile of the null (two-tailed) distribution.

The relationship between the center and surround of the horizontal receptive fields of neurons was calculated as the difference between the max evoked firing rate (or delta F) in the PWCZ and the max evoked firing rate in the AWCZ divided by their sum.

$$\text{Cent:Surr Index} = \frac{\max(\text{abs}(\text{PWCZ})) - \max(\text{abs}(\text{AWCZ}))}{\max(\text{abs}(\text{PWCZ})) + \max(\text{abs}(\text{AWCZ}))}$$

The spatial selectivity of neurons was calculated from the normed (Euclidean) vector of the peak normalized spatial tuning curves. This value was then divided by square root of *n* dimensions – 1 to restrict its range from 0 to 1. Larger values signify higher spatial selectivity (lower broadness). Raw spike rates were used.

$$\text{Spatial Selectivity} = 1 - \left(\frac{\frac{\|x\|}{max(x)} - 1}{\sqrt{n} - 1} \right)$$

Map analysis—Within each dataset, the centroids of all significantly driven and tuned ROIs were whitened and projected onto 1800 axes spanning from 0 to pi. The centroids of the ROIs were whitened to minimize spurious correlations derived from the structure of the ROIs sampled. A linear regression was computed between the projected location of the ROIs and their preferred positions (calculated over the entire tuning curve) for each axis. The axis of best fit was determined to be the axis whose linear regression had the largest r^2 value. This axis of best fit was then transformed into cortical space via the inverse of the whitening transform. The center of the axis was located to the center of the spared whisker column (as identified above) allowing for data across mice to be aggregated.

A Pearson's correlation was computed for the significantly driven and tuned neurons between their projected locations on the axis of best fit and their preferred positions, both before and after trimming. A linear regression was performed to compute the slope of that correlation. The mean pairwise correlation in tuning over the PWCZ (Pearson's R) was computed as a function of their pairwise difference of their projections along the axis of best fit and binned within 20 μm bins. Cumulative distribution functions were created by binning the location of the neurons along the projection into 18 equally sized bins. Only the central 8 bins, which had more than 145 neurons each (the expected value if the distribution of ROIs along the axis were uniform), are shown.

Quantification and Statistical Analysis

Statistically significant differences between conditions were determined using standard parametric or nonparametric tests in MATLAB, including a 1-way ANOVA, student's t-test, rank sum, and a Wilcoxon sign-rank test. Tests for normality were performed with a Lilliefors test. Units were defined as tuned for space if their evoked spike rate changed as a function of object position, determined by a 1-way ANOVA. Analysis of spatial preference changes was restricted to neurons that were significantly tuned for the stimulus both before and after trimming. The number of neurons that significantly changed their response per position was defined as neurons whose pre- and post-trimming response distributions were significantly different via a rank sum test. All "n" values are referring to the number of cells present in an analysis except when explicitly stated that the n is referring to the number of mice used.

Electrophysiology—Unless stated otherwise, analyses were performed from evoked spike rates. The spontaneous firing rate of a neuron in the 500 ms window preceding stimulation was subtracted from its firing rate of the last 500 ms of active touch, on a trial by trial basis. Neurons in L5 and the thalamus were classified as touch-facilitated or touch-suppressed. Touch facilitated neurons had a positive mean evoked spike rate in the principal whisker contact zone (PWCZ), while touch-suppressed neurons had a negative mean evoked rate in the PWCZ.

Two-photon calcium imaging—Analyses were performed on trial-wise dF/F. Analysis was limited to ROIs that met several criteria: they must be significantly driven by at least one stimulus, be larger than 50 μm^2, and for Figs. 2 and 3 have been within the principle whisker column. A significant response for a position had to meet two criteria: have a mean df/f greater than .2, and pass a t-test between the evoked responses at that position and the measured df/f values during control trials. The Benjamini & Hochberg false discovery rate correction was used to correct for the multiple comparisons taken across the multiple stimuli. Outlier responses per stimulus position were identified by the median rule, where values further than 2.3 times the inter-quartile range from the median are determined to be outliers, and were removed prior to any analysis. Neurons were identified to be within the spared principle whisker column or to be in a surrounding column by using a custom MATLAB (Mathworks) algorithm to segment the pixels that exhibited a significant response post-trimming (t-test between control trials and the mean of PWCZ stimulus trials) which is putatively localized to the spared column (Fig. S2). The neural response for a single trial was calculated as the average df/f during the last 500 ms of stimulation.

Supplementary Material

Refer to Web version on PubMed Central for supplementary material.

Acknowledgments

The authors acknowledge the GENIE Project, Janelia Farm Research Campus, Howard Hughes Medical Institute for the GCaMP6 viruses, as well as Dan Feldman and members of the Adesnik and Feldman labs for comments on the manuscript. H.A. is a New York Stem Cell Robertson Investigator. This work was supported by NINDS grant DP2NS087725-01 and the Whitehall Foundation.

References

Adesnik H, Bruns W, Taniguchi H, Huang ZJ, Scanziani M. A neural circuit for spatial summation in visual cortex. Nature. 2012; 490:226–231. [PubMed: 23060193]

Andermann ML, Moore CI. A somatotopic map of vibrissa motion direction within a barrel column. Nature neuroscience. 2006; 9:543–551. [PubMed: 16547511]

Andersen RA, Essick GK, Siegel RM. Encoding of spatial location by posterior parietal neurons. Science. 1985; 230:456–458. [PubMed: 4048942]

Armstrongjames M, Fox K, Dasgupta A. Flow of Excitation within Rat Barrel Cortex on Striking a Single Vibrissa. J Neurophysiol. 1992; 68:1345–1358. [PubMed: 1432088]

Bagdasarian K, Szwed M, Knutsen PM, Deutsch D, Derdikman D, Pietr M, Simony E, Ahissar E. Pre-neuronal morphological processing of object location by individual whiskers. Nature neuroscience. 2013; 16:622-+. [PubMed: 23563582]

Bandyopadhyay S, Shamma SA, Kanold PO. Dichotomy of functional organization in the mouse auditory cortex. Nature neuroscience. 2010; 13:361–368. [PubMed: 20118924]

Bender KJ, Allen CB, Bender VA, Feldman DE. Synaptic basis for whisker deprivation- induced synaptic depression in rat somatosensory cortex. Journal of Neuroscience. 2006; 26:4155–4165. [PubMed: 16624936]

Bender KJ, Rangel J, Feldman DE. Development of columnar topography in the excitatory layer 4 to layer 2/3 projection in rat barrel cortex. Journal of Neuroscience. 2003; 23:8759–8770. [PubMed: 14507976]

Boloori AR, Stanley GB. The dynamics of spatiotemporal response integration in the somatosensory cortex of the vibrissa system. Journal of Neuroscience. 2006; 26:3767–3782. [PubMed: 16597730]

Brecht M. Barrel cortex and whisker-mediated behaviors. Curr Opin Neurobiol. 2007; 17:408–416. [PubMed: 17702566]

Brecht M, Roth A, Sakmann B. Dynamic receptive fields of reconstructed pyramidal cells in layers 3 and 2 of rat somatosensory barrel cortex. J Physiol-London. 2003; 553:243–265. [PubMed: 12949232]

Brecht M, Sakmann B. Dynamic representation of whisker deflection by synaptic potentials in spiny stellate and pyramidal cells in the barrels and septa of layer 4 rat somatosensory cortex. J Physiol-London. 2002; 543:49–70. [PubMed: 12181281]

Brown AW, Waite PM. Responses in the rat thalamus to whisker movements produced by motor nerve stimulation. The Journal of physiology. 1974; 238:387–401. [PubMed: 4840852]

Brumberg JC, Pinto DJ, Simons DJ. Spatial gradients and inhibitory summation in the rat whisker barrel system. J Neurophysiol. 1996; 76:130–140. [PubMed: 8836214]

Brumberg JC, Pinto DJ, Simons DJ. Cortical columnar processing in the rat whisker-to-barrel system. J Neurophysiol. 1999; 82:1808–1817. [PubMed: 10515970]

Castro-Alamancos MA. Absence of rapid sensory adaptation in neocortex during information processing states. Neuron. 2004a; 41:455–464. [PubMed: 14766183]

Castro-Alamancos MA. Dynamics of sensory thalamocortical synaptic networks during information processing states. Progress in neurobiology. 2004b; 74:213–247. [PubMed: 15556288]

Castro-Alamancos MA, Bezdudnaya T. Modulation of artificial whisking related signals in barrel cortex. J Neurophysiol. 2015; 113:1287–1301. [PubMed: 25505118]

Castro-Alamancos MA, Oldford E. Cortical sensory suppression during arousal is due to the activity-dependent depression of thalamocortical synapses. J Physiol-London. 2002; 541:319–331. [PubMed: 12015438]

Chapman CE, Ageranioti-Belanger SA. Discharge properties of neurones in the hand area of primary somatosensory cortex in monkeys in relation to the performance of an active tactile discrimination task. I. Areas 3b and 1. Exp Brain Res. 1991; 87:319–339. [PubMed: 1769386]

Chen-Bee CH, Zhou Y, Jacobs NS, Lim B, Frostig RD. Whisker array functional representation in rat barrel cortex: transcendence of one-to-one topography and its underlying mechanism. Front Neural Circuits. 2012; 6:93. [PubMed: 23205005]

Chen TW, Wardill TJ, Sun Y, Pulver SR, Renninger SL, Baohan A, Schreiter ER, Kerr RA, Orger MB, Jayaraman V, et al. Ultrasensitive fluorescent proteins for imaging neuronal activity. Nature. 2013; 499:295–300. [PubMed: 23868258]

Civillico EF, Contreras D. Integration of evoked responses in supragranular cortex studied with optical recordings in vivo. J Neurophysiol. 2006; 96:336–351. [PubMed: 16571736]

Clancy KB, Schnepel P, Rao AT, Feldman DE. Structure of a single whisker representation in layer 2 of mouse somatosensory cortex. The Journal of neuroscience : the official journal of the Society for Neuroscience. 2015; 35:3946–3958. [PubMed: 25740523]

Crochet S, Poulet JF, Kremer Y, Petersen CC. Synaptic mechanisms underlying sparse coding of active touch. Neuron. 2011; 69:1160–1175. [PubMed: 21435560]

Curtis JC, Kleinfeld D. Phase-to-rate transformations encode touch in cortical neurons of a scanning sensorimotor system. Nature neuroscience. 2009; 12:492–501. [PubMed: 19270688]

Diamond ME, von Heimendahl M, Knutsen PM, Kleinfeld D, Ahissar E. 'Where' and 'what' in the whisker sensorimotor system (vol 9, pg 601, 2008). Nat Rev Neurosci. 2008; 9:I–I.

Drew PJ, Feldman DE. Representation of moving wavefronts of whisker deflection in rat somatosensory cortex. J Neurophysiol. 2007; 98:1566–1580. [PubMed: 17567777]

Ego-Stengel V, Mello e Souza T, Jacob V, Shulz DE. Spatiotemporal characteristics of neuronal sensory integration in the barrel cortex of the rat. J Neurophysiol. 2005; 93:1450–1467. [PubMed: 15496491]

Estebanez L, Bertherat J, Shulz DE, Bourdieu L, Leger JF. A radial map of multi-whisker correlation selectivity in the rat barrel cortex. Nat Commun. 2016; 7

Estebanez L, El Boustani S, Destexhe A, Shulz DE. Correlated input reveals coexisting coding schemes in a sensory cortex. Nature neuroscience. 2012; 15:1691-+. [PubMed: 23160042]

Fanselow EE, Nicolelis MAL. Behavioral modulation of tactile responses in the rat somatosensory system. Journal of Neuroscience. 1999; 19:7603–7616. [PubMed: 10460266]

Feldman DE, Brecht M. Map plasticity in somatosensory cortex. Science. 2005; 310:810–815. [PubMed: 16272113]

Feldmeyer D, Brecht M, Helmchen F, Petersen CC, Poulet JF, Staiger JF, Luhmann HJ, Schwarz C. Barrel cortex function. Progress in neurobiology. 2013; 103:3–27. [PubMed: 23195880]

Ferezou I, Haiss F, Gentet LJ, Aronoff R, Weber B, Petersen CCH. Spatiotemporal dynamics of cortical sensorimotor integration in behaving mice. Neuron. 2007; 56:907–923. [PubMed: 18054865]

Fox K. Anatomical pathways and molecular mechanisms for plasticity in the barrel cortex. Neuroscience. 2002; 111:799–814. [PubMed: 12031405]

Ghazanfar AA, Nicolelis MA. Spatiotemporal properties of layer V neurons of the rat primary somatosensory cortex. Cereb Cortex. 1999; 9:348–361. [PubMed: 10426414]

Glazewski S, Fox K. Time course of experience-dependent synaptic potentiation and depression in barrel cortex of adolescent rats. J Neurophysiol. 1996; 75:1714–1729. [PubMed: 8727408]

Goldreich D, Kyriazi HT, Simons DJ. Functional independence of layer IV barrels in rodent somatosensory cortex. J Neurophysiol. 1999; 82:1311–1316. [PubMed: 10482750]

Greenberg DS, Houweling AR, Kerr JND. Population imaging of ongoing neuronal activity in the visual cortex of awake rats. Nature neuroscience. 2008; 11:749–751. [PubMed: 18552841]

Hartline HK, Wagner HG, Ratliff F. Inhibition in the Eye of Limulus. J Gen Physiol. 1956; 39:651–673. [PubMed: 13319654]

Hartmann MJ. A night in the life of a rat: vibrissal mechanics and tactile exploration. Annals of the New York Academy of Sciences. 2011; 1225:110–118. [PubMed: 21534998]

Hentschke H, Haiss F, Schwarz C. Central signals rapidly switch tactile processing in rat barrel cortex during whisker movements. Cerebral Cortex. 2006; 16:1142–1156. [PubMed: 16221924]

Higley MJ, Contreras D. Nonlinear integration of sensory responses in the rat barrel cortex: an intracellular study in vivo. The Journal of neuroscience : the official journal of the Society for Neuroscience. 2003; 23:10190–10200. [PubMed: 14614077]

Hill DN, Mehta SB, Kleinfeld D. Quality Metrics to Accompany Spike Sorting of Extracellular Signals. Journal of Neuroscience. 2011; 31:8699–8705. [PubMed: 21677152]

Hirata A, Castro-Alamancos MA. Cortical transformation of wide-field (multiwhisker) sensory responses. J Neurophysiol. 2008; 100:358–370. [PubMed: 18480364]

Hires SA, Gutnisky DA, Yu JN, O'Connor DH, Svoboda K. Low-noise encoding of active touch by layer 4 in the somatosensory cortex. Elife. 2015; 4

Hobbs JA, Towal RB, Hartmann MJZ. Spatiotemporal Patterns of Contact Across the Rat Vibrissal Array During Exploratory Behavior. Front Behav Neurosci. 2016; 9

Jacob V, Le Cam J, Ego-Stengel V, Shulz DE. Emergent Properties of Tactile Scenes Selectively Activate Barrel Cortex Neurons. Neuron. 2008; 60:1112–1125. [PubMed: 19109915]

Kelly MK, Carvell GE, Kodger JM, Simons DJ. Sensory loss by selected whisker removal produces immediate disinhibition in the somatosensory cortex of behaving rats. The Journal of neuroscience : the official journal of the Society for Neuroscience. 1999; 19:9117–9125. [PubMed: 10516329]

Kleinfeld D, Ahissar E, Diamond ME. Active sensation: insights from the rodent vibrissa sensorimotor system. Curr Opin Neurobiol. 2006; 16:435–444. [PubMed: 16837190]

Knudsen EI, du Lac S, Esterly SD. Computational maps in the brain. Annual review of neuroscience. 1987; 10:41–65.

Knutsen PM, Biess A, Ahissar E. Vibrissal kinematics in 3D: tight coupling of azimuth, elevation, and torsion across different whisking modes. Neuron. 2008; 59:35–42. [PubMed: 18614027]

Knutsen PM, Pietr M, Ahissar E. Haptic object localization in the vibrissal system: behavior and performance. The Journal of neuroscience : the official journal of the Society for Neuroscience. 2006; 26:8451–8464. [PubMed: 16914670]

Kremer Y, Leger JF, Goodman D, Brette R, Bourdieu L. Late Emergence of the Vibrissa Direction Selectivity Map in the Rat Barrel Cortex. Journal of Neuroscience. 2011; 31:10689–10700. [PubMed: 21775612]

Krupa DJ, Matell MS, Brisben AJ, Oliveira LM, Nicolelis MA. Behavioral properties of the trigeminal somatosensory system in rats performing whisker-dependent tactile discriminations. The Journal of neuroscience : the official journal of the Society for Neuroscience. 2001; 21:5752–5763. [PubMed: 11466447]

Kuffler SW. Discharge Patterns and Functional Organization of Mammalian Retina. J Neurophysiol. 1953; 16:37–68. [PubMed: 13035466]

Kwegyir-Afful EE, Bruno RM, Simons DJ, Keller A. The role of thalamic inputs in surround receptive fields of barrel neurons. The Journal of neuroscience : the official journal of the Society for Neuroscience. 2005; 25:5926–5934. [PubMed: 15976081]

Lee S, Carvell GE, Simons DJ. Motor modulation of afferent somatosensory circuits. Nature neuroscience. 2008; 11:1430–1438. [PubMed: 19011625]

Lee S, Kruglikov I, Huang ZJ, Fishell G, Rudy B. A disinhibitory circuit mediates motor integration in the somatosensory cortex. Nature neuroscience. 2013; 16:1662–1670. [PubMed: 24097044]

Madisen L, Zwingman TA, Sunkin SM, Oh SW, Zariwala HA, Gu H, Ng LL, Palmiter RD, Hawrylycz MJ, Jones AR, et al. A robust and high-throughput Cre reporting and characterization system for the whole mouse brain. Nature neuroscience. 2010; 13:133–U311. [PubMed: 20023653]

Mirabella G, Battiston S, Diamond ME. Integration of multiple-whisker inputs in rat somatosensory cortex. Cereb Cortex. 2001; 11:164–170. [PubMed: 11208671]

Moore CI, Nelson SB. Spatio-temporal subthreshold receptive fields in the vibrissa representation of rat primary somatosensory cortex. J Neurophysiol. 1998; 80:2882–2892. [PubMed: 9862892]

Moore CI, Nelson SB, Sur M. Dynamics of neuronal processing in rat somatosensory cortex. Trends Neurosci. 1999; 22:513–520. [PubMed: 10529819]

Niell CM, Stryker MP. Modulation of Visual Responses by Behavioral State in Mouse Visual Cortex. Neuron. 2010; 65:472–479. [PubMed: 20188652]

O'Connor DH, Clack NG, Huber D, Komiyama T, Myers EW, Svoboda K. Vibrissa-based object localization in head-fixed mice. The Journal of neuroscience : the official journal of the Society for Neuroscience. 2010a; 30:1947–1967. [PubMed: 20130203]

O'Connor DH, Peron SP, Huber D, Svoboda K. Neural Activity in Barrel Cortex Underlying Vibrissa-Based Object Localization in Mice. Neuron. 2010b; 67:1048–1061. [PubMed: 20869600]

Oberlaender M, Ramirez A, Bruno RM. Sensory experience restructures thalamocortical axons during adulthood. Neuron. 2012; 74:648–655. [PubMed: 22632723]

Ohki K, Chung S, Ch'ng YH, Kara P, Reid RC. Functional imaging with cellular resolution reveals precise micro-architecture in visual cortex. Nature. 2005; 433:597–603. [PubMed: 15660108]

Peron SP, Freeman J, Iyer V, Guo C, Svoboda K. A Cellular Resolution Map of Barrel Cortex Activity during Tactile Behavior. Neuron. 2015; 86:783–799. [PubMed: 25913859]

Petersen CCH. The functional organization of the barrel cortex. Neuron. 2007; 56:339–355. [PubMed: 17964250]

Petersen RS, Panzeri S, Diamond ME. Population coding of stimulus location in rat somatosensory cortex. Neuron. 2001; 32:503–514. [PubMed: 11709160]

Pluta S, Naka A, Veit J, Telian G, Yao L, Hakim R, Taylor D, Adesnik H. A direct translaminar inhibitory circuit tunes cortical output. Nature neuroscience. 2015; 18:1631–1640. [PubMed: 26414615]

Poulet JF, Petersen CC. Internal brain state regulates membrane potential synchrony in barrel cortex of behaving mice. Nature. 2008; 454:881–885. [PubMed: 18633351]

Ramirez A, Pnevmatikakis EA, Merel J, Paninski L, Miller KD, Bruno RM. Spatiotemporal receptive fields of barrel cortex revealed by reverse correlation of synaptic input. Nature neuroscience. 2014; 17:866–875. [PubMed: 24836076]

Reimer J, Froudarakis E, Cadwell CR, Yatsenko D, Denfield GH, Tolias AS. Pupil fluctuations track fast switching of cortical states during quiet wakefulness. Neuron. 2014; 84:355–362. [PubMed: 25374359]

Ringach DL, Mineault PJ, Tring E, Olivas ND, Garcia-Junco-Clemente P, Trachtenberg JT. Spatial clustering of tuning in mouse primary visual cortex. Nat Commun. 2016; 7

Rothschild G, Nelken I, Mizrahi A. Functional organization and population dynamics in the mouse primary auditory cortex. Nature neuroscience. 2010; 13:353–360. [PubMed: 20118927]

Sato TR, Gray NW, Mainen ZF, Svoboda K. The functional microarchitecture of the mouse barrel cortex. Plos Biol. 2007; 5:1440–1452.

Shimegi S, Akasaki T, Ichikawa T, Sato H. Physiological and anatomical organization of multiwhisker response interactions in the barrel cortex of rats. The Journal of neuroscience : the official journal of the Society for Neuroscience. 2000a; 20:6241–6248. [PubMed: 10934274]

Shimegi S, Akasaki T, Ichikawa T, Sato H. Physiological and anatomical organization of multiwhisker response interactions in the barrel cortex of rats. Journal of Neuroscience. 2000b; 20:6241–6248. [PubMed: 10934274]

Smith SL, Hausser M. Parallel processing of visual space by neighboring neurons in mouse visual cortex. Nature neuroscience. 2010; 13:1144–1149. [PubMed: 20711183]

Sofroniew NJ, Cohen JD, Lee AK, Svoboda K. Natural whisker-guided behavior by head-fixed mice in tactile virtual reality. The Journal of neuroscience : the official journal of the Society for Neuroscience. 2014; 34:9537–9550. [PubMed: 25031397]

Szwed M, Bagdasarian K, Ahissar E. Encoding of vibrissal active touch. Neuron. 2003; 40:621–630. [PubMed: 14642284]

Timofeeva E, Lavallee P, Arsenault D, Deschenes M. Synthesis of multiwhisker-receptive fields in subcortical stations of the vibrissa system. J Neurophysiol. 2004; 91:1510–1515. [PubMed: 14668302]

Vinck M, Batista-Brito R, Knoblich U, Cardin JA. Arousal and Locomotion Make Distinct Contributions to Cortical Activity Patterns and Visual Encoding. Neuron. 2015; 86:740–754. [PubMed: 25892300]

Wallach A, Bagdasarian K, Ahissar E. On-going computation of whisking phase by mechanoreceptors. Nature neuroscience. 2016; 19:487-+. [PubMed: 26780508]

Wen JA, DeBlois MC, Barth AL. Initiation, Labile, and Stabilization Phases of Experience-Dependent Plasticity at Neocortical Synapses. Journal of Neuroscience. 2013; 33:8483–8493. [PubMed: 23658185]

Woolsey TA, Van der Loos H. The structural organization of layer IV in the somatosensory region (SI) of mouse cerebral cortex. The description of a cortical field composed of discrete cytoarchitectonic units. Brain research. 1970; 17:205–242. [PubMed: 4904874]

Yang AET, Hartmann MJZ. Whisking Kinematics Enables Object Localization in Head-Centered Coordinates Based on Tactile Information from a Single Vibrissa. Front Behav Neurosci. 2016; 10

Yu CX, Horev G, Rubin N, Derdikman D, Haidarliu S, Ahissar E. Coding of Object Location in the Vibrissal Thalamocortical System. Cerebral Cortex. 2015; 25:563–577. [PubMed: 24062318]

Zhu JJ, Connors BW. Intrinsic firing patterns and whisker-evoked synaptic responses of neurons in the rat barrel cortex. J Neurophysiol. 1999; 81:1171–1183. [PubMed: 10085344]

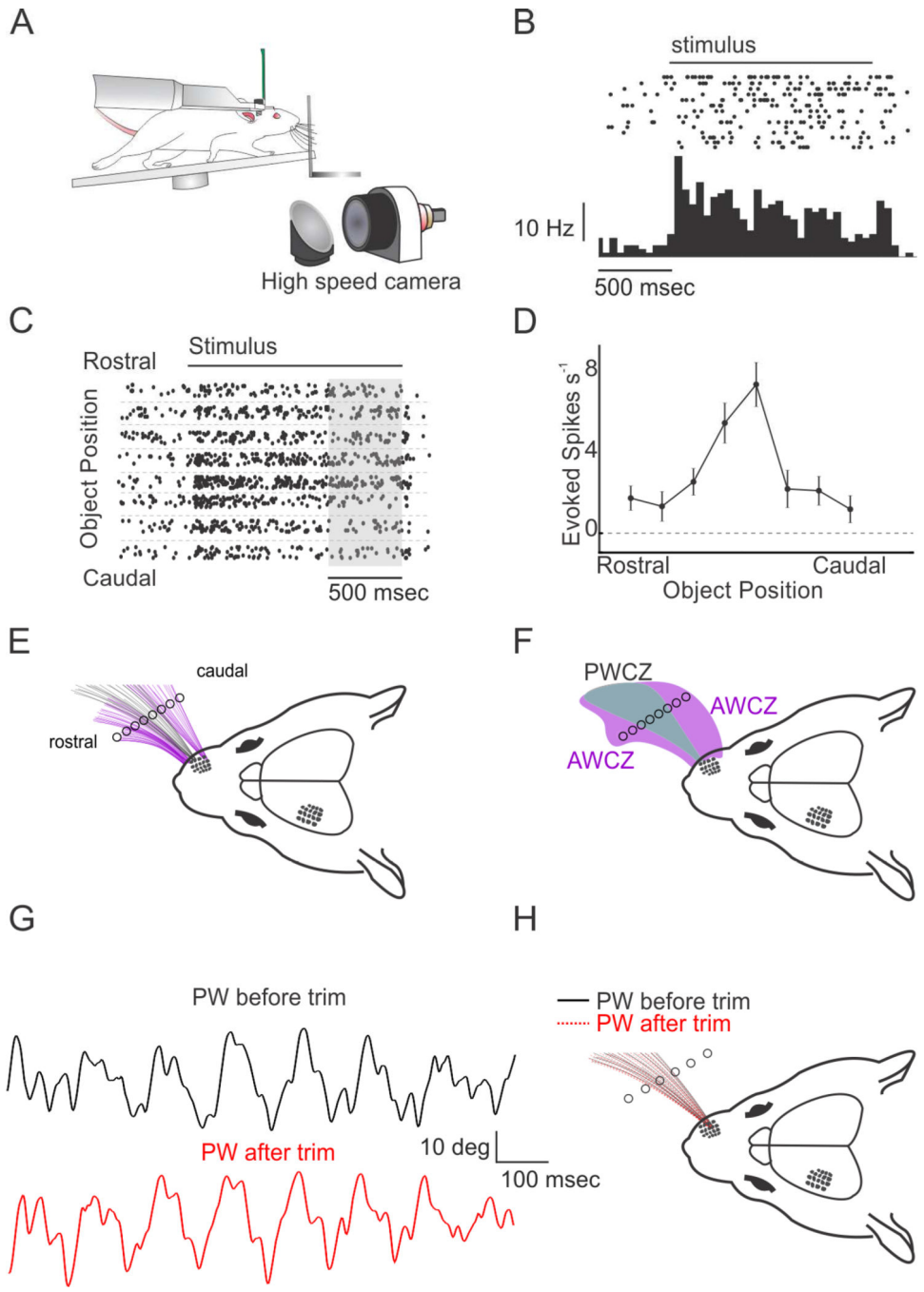

Figure 1. Probing the cortical representation of scanned space in the whisker system

A) Experimental schematic: a head-fixed mouse runs on a circular treadmill, while a vertical bar is moved to different locations along the horizontal whisking axis. A high speed camera captures movements of the whiskers. B) An example raster plot (top) and PSTH (bottom) of a cortical L5 unit in response to touch with the stimulus bar at its preferred location. C) Raster plot for the same unit for several trials across each of the 8 positions probed. The grey rectangle indicates the time window for analysis of neural data. D) Tuning curve (mean ± s.e.m.) for this example unit. E) Plot of the whisker positions across the full range of

protraction for four tracked whiskers (during free whisking) overlaid on a schematic of the animal's head. Grey: the selected principal whisker (C2). Purple: the adjacent whiskers of the C row. F) Diagram of the zone swept out by the principal whisker (PWCZ, red) and the adjacent whiskers of the same row (AWCZ, purple). G) Example traces of the principal whisker's (C2) movement along the horizontal axis before (black) and after (red) trimming all but the C2 whisker. H) Example plot of the PW's movement before (black) and after (red) trimming all but the C2 whisker. Red and black traced whisker positions are overlaid.

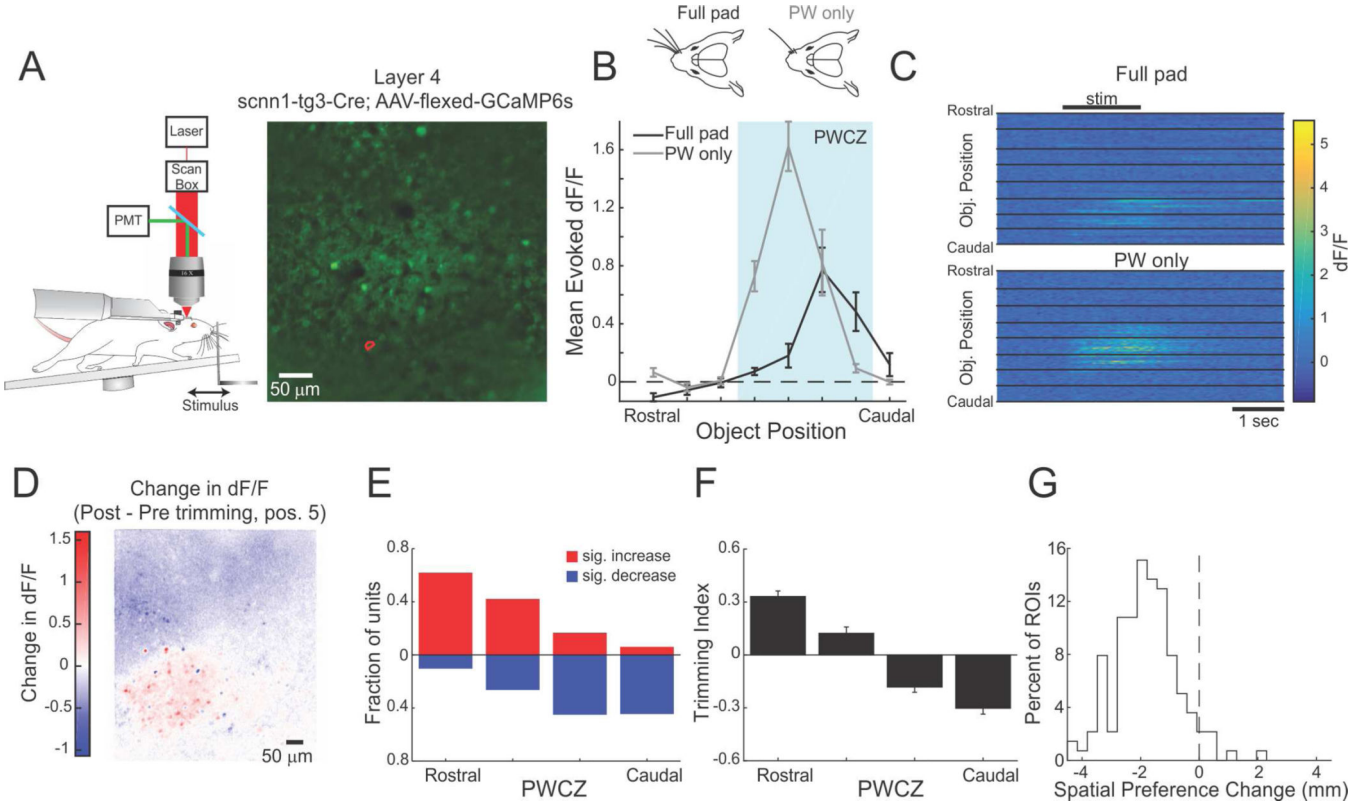

Figure 2. Surround whisker input powerfully modulates spatial representations in L4 excitatory neurons

A) Left: experimental schematic of a head-fixed mouse under a two photon microscope. Right: Example image of GCaMP6s-expressing L4 excitatory neurons. The C2 barrel is at center. The red outline indicates the position of the example neuron in B,C. B) Top: schematic of the pre- and post-surround whisker trimming conditions. Bottom: Example tuning curve (mean ± s.e.m.) of a single L4 neuron before (black) and after (grey) trimming all but the C2 whisker. C) Example 'raster' plot of calcium responses of the neuron from B). Top: before trimming. Bottom: after trimming. Responses from all eight stimulus positions are presented in both cases. D) Example image of the mean change in dF/F for each neuron in the field of view in L4 between post and pre trimming conditions for stimulus position five. Red indicates an increase in mean evoked responses, blue indicates a decrease. A Gaussian blur was applied. E) Plot of the fraction of cells in the C2 barrel that show significant increases (red) or decreases (blue) across each of the four stimulus positions within the PWCZ (n = 231 cells in 3 mice). F) Plot of the average trimming index for the same cells across the same stimulus conditions. G) Histogram of the change in spatial preference for all imaged neurons in the C2 barrel that exhibited significant spatial tuning both before and after surround whisker trimming (n = 139 cells across 3 mice, $p < 0.001$, t-test).

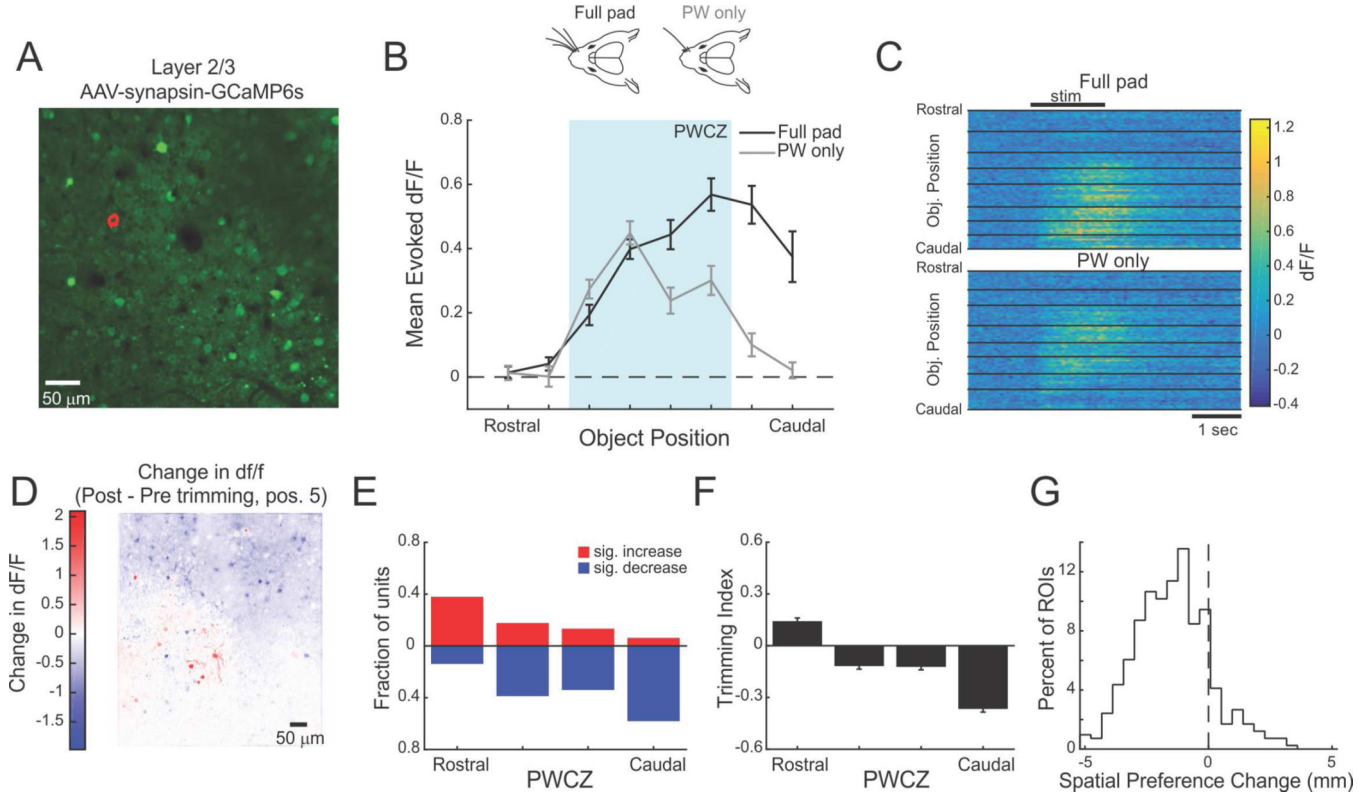

Figure 3. Spatial summation in L2/3 neurons

A) Example image of GCaMP6s-expressing L2/3 neurons. The anatomic aligned C2 column is at center. The red outline indicates the position of the example neuron in B, C. B) Top: schematic of the pre- and post-surround whisker trimming conditions. Bottom: Example tuning curve (mean ± s.e.m.) of a single L2/3 neuron before (black) and after (grey) trimming all but the C2 whisker. C) Example 'raster' plot of calcium responses of the cell from B). Top: before trimming. Bottom: after trimming. Responses from all 8 stimulus positions are presented in both cases. D) Example image of the mean change in dF/F for each neuron in the field of view in L2/3 between post and pre trimming conditions for stimulus position 5. Red indicates an increase in mean evoked responses, blue indicates a decrease. A Gaussian blur was applied. E) Plot of the fraction of cells in the C2 barrel that show significant increases (red) or decreases (blue) across each of the four stimulus positions within the PWCZ (n = 631 cells in 4 mice). F) Plot of the average trimming index for the same cells across the same stimulus conditions. G) Histogram of the change in spatial preference for all imaged neurons in the C2 column that exhibited significant spatial tuning both before and after surround whisker trimming (n = 413 cells across 4 mice, $p < 0.001$, Wilcoxon sign rank).

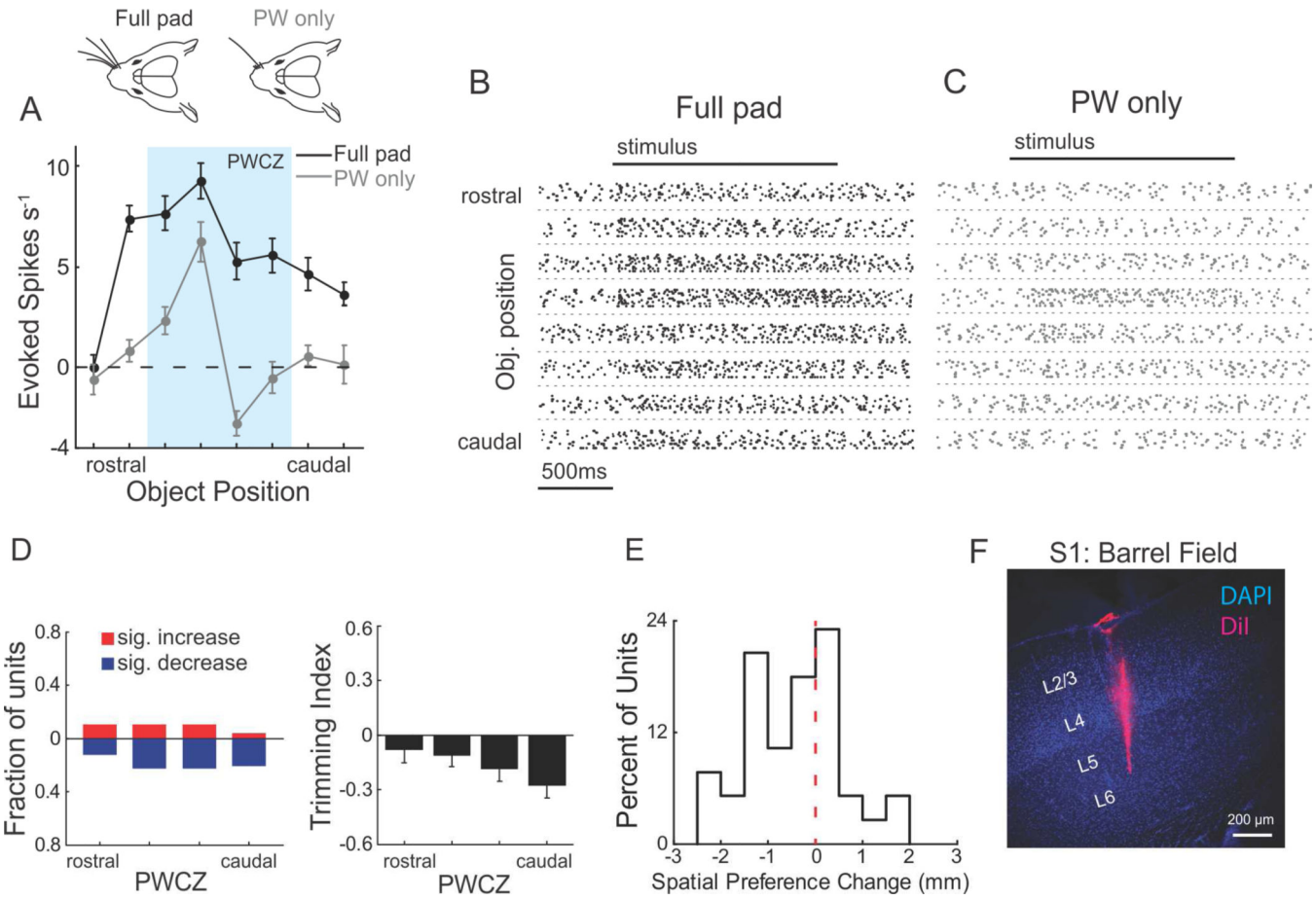

Figure 4. Spatial summation in touch responsive regular spiking units of L5

A) Top: schematic of the pre- and post-surround whisker trimming conditions. Bottom: Example tuning curve (mean ± s.e.m.) of a single L5 RS unit before (black) and after (grey) trimming all but the principal whisker. B) Example raster of the unit from A) before trimming to the principal whisker. C) As in B) but for after trimming. Responses from all 8 stimulus positions are presented in both cases. D) Left: Plot of the fraction of L5 RS units in the spared whisker column that show significant increases (red) or decreases (blue) across each of the four stimulus positions within the PWCZ. Right: Plot of the average trimming index for the same cells across the same stimulus conditions (n = 48 units in 8 mice). E) Histogram of the change in spatial preference for all recorded L5 RS units in the spared column with significant spatial tuning both before and after surround whisker trimming (n = 39 units across 8 mice, p = 0.001, Wilcoxon). F) Example image from a recorded animal showing the DiI track (red) of the multi-electrode array extending into L5.

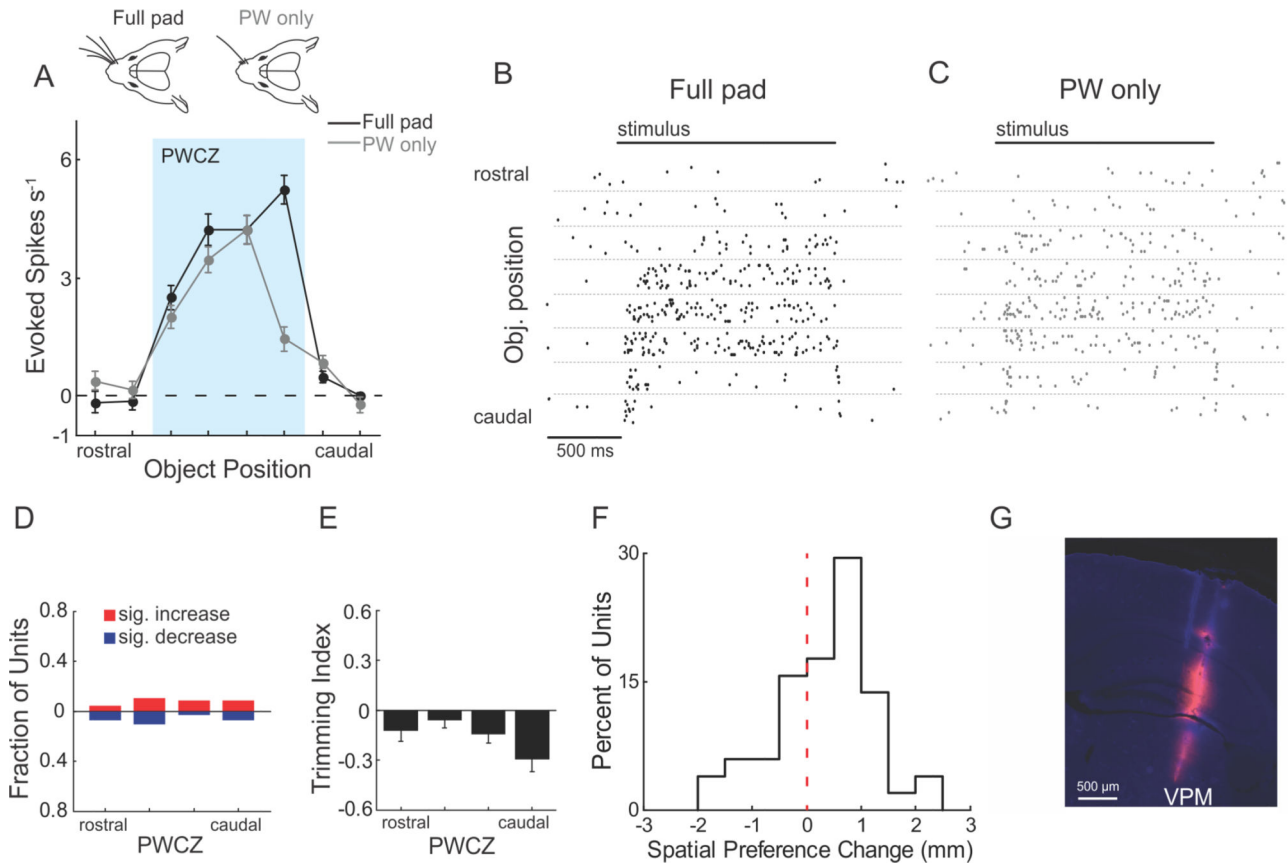

Figure 5. Weak surround modulation in thalamic neurons in VPM

A) Top: schematic of the pre- and post-surround whisker trimming conditions. Bottom: Example tuning curve (mean ± s.e.m.) of a single VPM unit before (black) and after (grey) trimming all but the C2 whisker. B) Example raster of the unit from A) before trimming to the C2 whisker. C) As in B) but for after trimming. Responses from all 8 stimulus positions are presented in both cases. D) Plot of the fraction of units in the C2 barreloid that show significant increases (blue) or decreases (red) across each of the four stimulus positions within the PWCZ (n = 54 units across 8 mice). E) Plot of the average trimming index for the same cells across the same stimulus conditions. F) Histogram of the change in spatial preference for all recorded units in the C2 barreloid with significant spatial tuning both before and after surround whisker trimming (n = 51 units across 8 mice, p = 0.23, paired t-test). G) Example image form a recorded animal showing the DiI track (red) of the multi-electrode array extending into VPM.

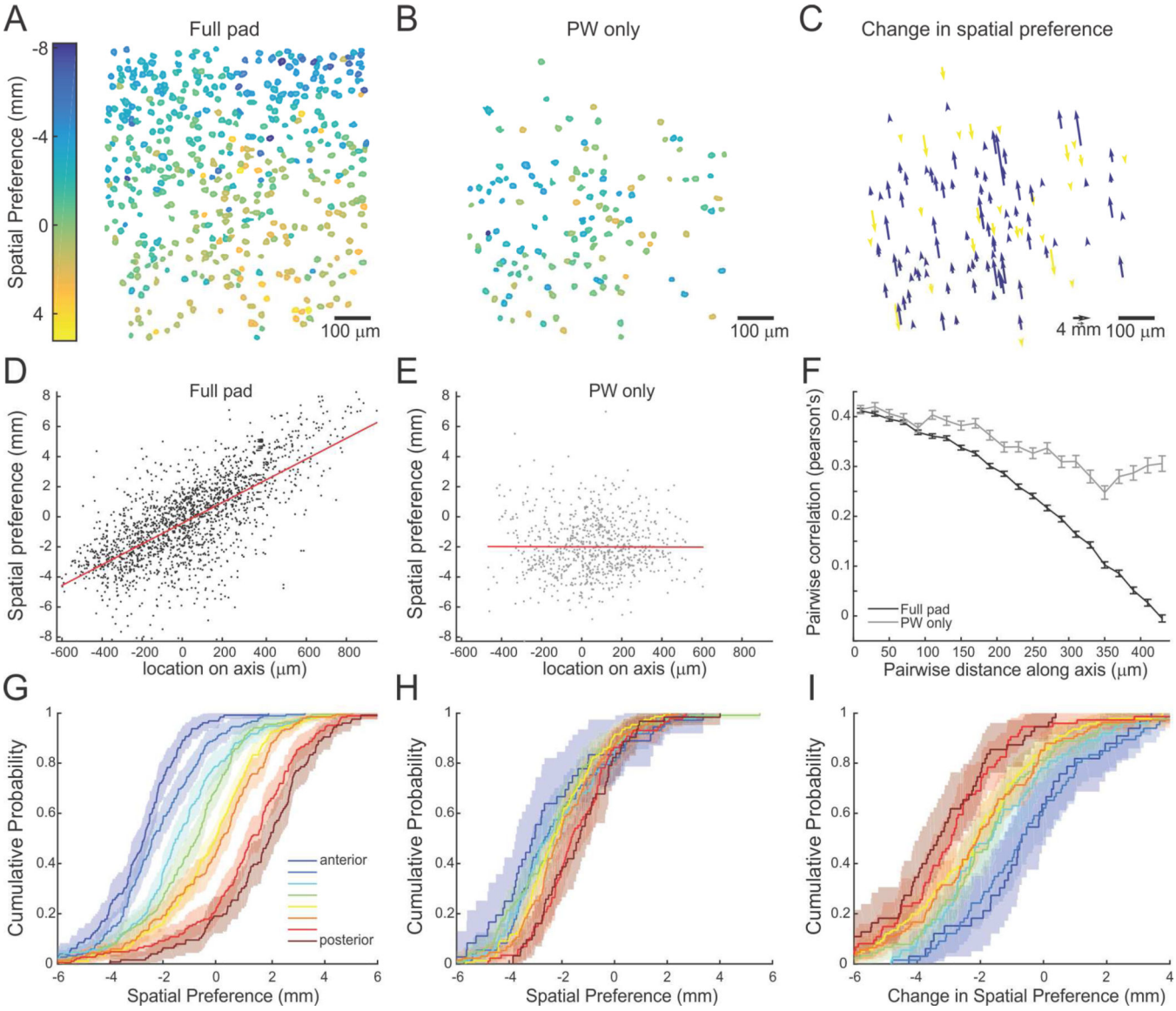

Figure 6. Surround whiskers organize a spatial map in L2/3 of the barrel cortex

A) Example spatial preference map in a mouse with all the whiskers intact of a field of view in L2/3 imaged with two photon microscopy. The color indicates the spatial preference of the stimulus bar's position. Only neurons that exhibited significant activity and spatial tuning are shown. B) Same field of view as in A) but collected immediately after removing all but the C2 whisker. Again, only neurons that exhibited significant activity and spatial tuning are shown. C) Plot of the magnitude and direction of change in spatial preference for all imaged neurons within A) and B) that exhibited significant spatial tuning both before and after surround whisker trimming. Yellow: rostral shift, purples: caudal shift. The length of each arrow corresponds to the magnitude of change in spatial preference, and its direction indicates the sign of the change. The arrows are all aligned to the axis of best fit for preferred position calculated prior to trimming. D) Plot of the spatial preference of all significantly tuned L2/3 cells versus their position along the axis of best fit (1789 neurons, 4

mice). The red line is a linear regression to the data. E) As in D) but for after trimming to the C2 whisker (796 neurons, 4 mice). F) Binned plot of the pairwise correlation of spatial tuning curves for all pairs of significantly tuned L2/3 neurons within each mouse as a function of distance in cortical space. G) Cumulative distribution plots of spatial preference of significantly driven and tuned neurons before trimming as a function of cortical position along the axis of best fit. H) As in G) but for after trimming to the C2 whisker. I) Cumulative distribution plot of the change in spatial preference for all the recorded neurons.

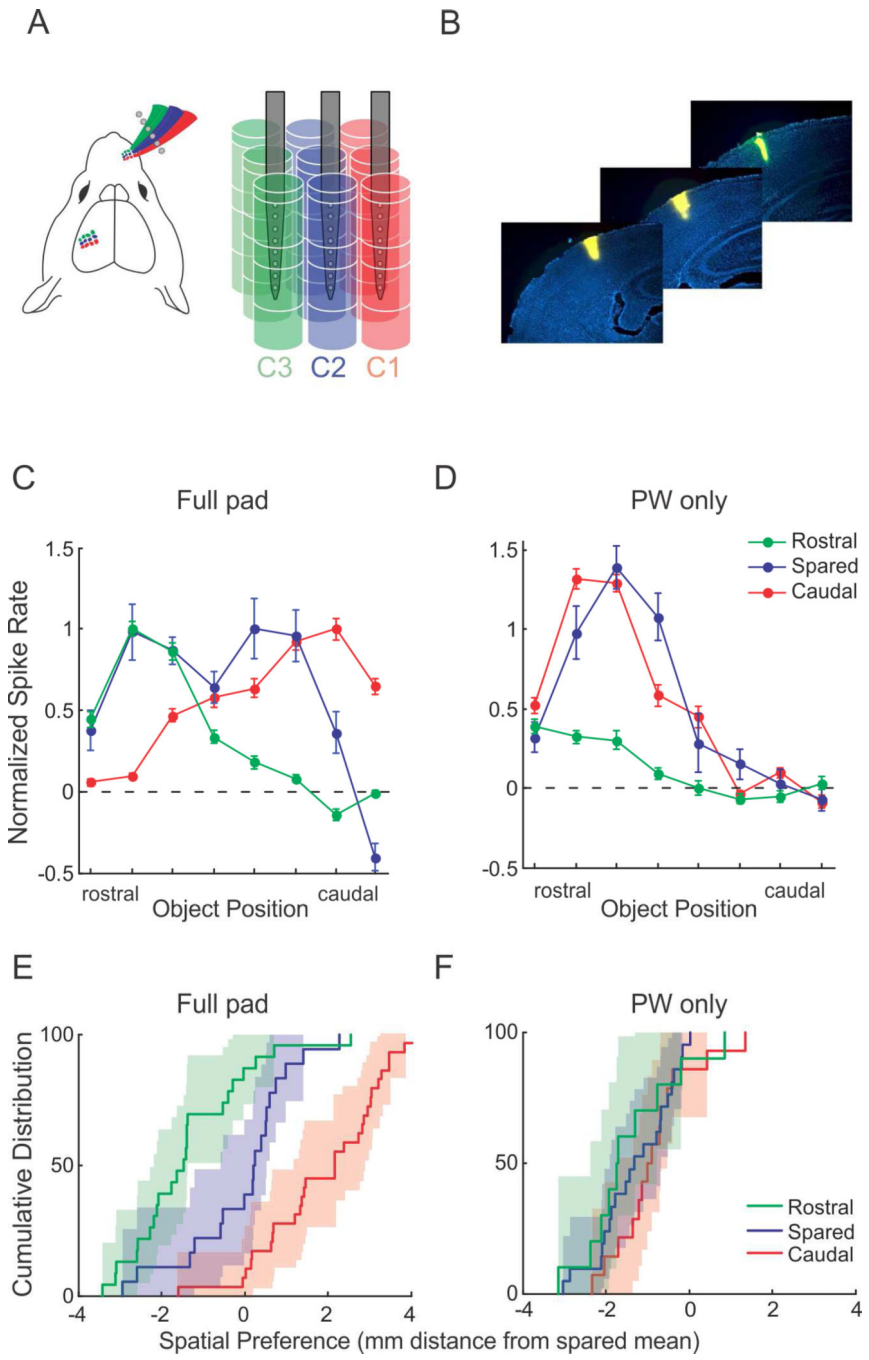

Figure 7. Surround whiskers distribute spatial representations in L5

A) Schematic of multi-shank laminar recordings in L5. B) Example histological images of the electrode of three adjacent shanks in S1. C) Example spatial tuning curves from three units on three adjacent electrode shanks. D) As in C) but following trimming off the surround whiskers. E) Cumulative distribution plots of spatial preference of significantly tuned units on each electrode shank before trimming. F) As in E) but following trimming off the surround whiskers.